High Energy Physics and Nuclear Physics

Volume 13, No.1

Study of Associated Gamma Rays from Niobium under 14.9 MeV Neutron Bombardments

Zhou Hongyu, Yan Yiming, Fan Guoying, Lan Liqiao, Wang Qi, Sun Shuxu, Hua Ming, Han Chongzhan, Liu Shuzhen, Rong Yaning, Wen Shenlin, Wang Xinfu, Yan Hua and Wang Wanhong[1]; and Tang Lin[2]

([1]Institute of Low Energy Nuclear Physics, Beijing Normal University)
([2]Department of Mathematical and Physical Science, National Natural Science Foundation of China, Beijing)

The gamma-ray spectra from niobium under 14.9 MeV neutron bombardments were measured by means of a pulsed $T(d, n)^4$He neutron source, associated particle method, Ge(Li) detector and time-of-flight technique at 7 angles between 30° and 140°. 79 gamma-lines were determined by a high resolution gamma-spectrum analysis program. The reaction types and the transition levels of 62 lines were preliminarily assigned. Of the 79 gamma-lines, 40 lines were first found in the reactions induced by neutrons. The differential cross sections of every gamma-line at 7 angles were determined. Our study shows that the associated gamma-ray emissions from this reaction are basically isotropic.

1. INTRODUCTION

Following the progress of modern science and technology people believe more and more that the energies released by the thermonuclear fusion reactions must become an inexhaustible new energy source in the future. Since metal niobium will play an important role in the development and utilization of this new energy source because of its excellent physical and chemical properties, it

Supported by the Nationa Natural Science Foundation of China and Ministry of Nuclear Industry of China.
Received on Decembe 23, 1987.

might be one of the most ideal materials used for plasma compression in fusion reactor construction. This consideration has stimulated the interests of the study for the interactions of fast neutron (up to 14 MeV energies and above) with niobium [1,2]. The discrete gamma-ray spectra, differential production cross sections and angular distributions in the interactions are the basic nuclear data for fusion reactor designs. In addition, these data can also provide valuable knowledge for the studies of nuclear structure and nuclear reaction mechanism. Some earlier researches were focused in 0.6—3.0 MeV neutron energy range [3—6], and they aimed at studying the level structure of ^{93}Nb. Because of the requirements of fusion reactor designs the interests were progressively transferred to the studies of 14 MeV neutron energy in recent years [7,8]. But due to the larger level density of Nb and the lower gamma-ray yield induced by 14 neutrons, previous studies of the discrete gamma-ray spectra were performed only at limited number of angles, no report about the systematic angular distribution study has been seen so far. In the present work a Ge(Li) detector with higher detection efficiency and energy resolution was used, and the discrete gamma-ray spectra and the differential production cross sections for the reaction of 14.9 MeV neutrons with niobium sample at 7 angles between 30° and 140° were first measured.

2. EXPERIMENTAL PRINCIPLE AND METHOD

The gamma-rays in the interactions of 14.9 MeV neutrons with niobium mainly come from reaction channels $(n, n'\gamma)$, $(n, 2n\gamma)$, and so on. The differential production cross section of a discrete gamma-ray with energy E_γ at angle θ with respect to the incident neutron direction can be determined by the following formula:

$$\frac{d\sigma}{d\Omega}(E_\gamma, \theta) = \frac{N_\gamma(E_\gamma, \theta)}{4\pi\phi_n N\varepsilon(E_\gamma)} f, \tag{1}$$

where ϕ_n is the number of neutrons incident upon the sample, $N_\gamma(E_\gamma, \theta)$ is the count in the full energy peak of the gamma- line with energy E_γ detected at θ-direction, $\varepsilon(E_\gamma)$ the absolute detection

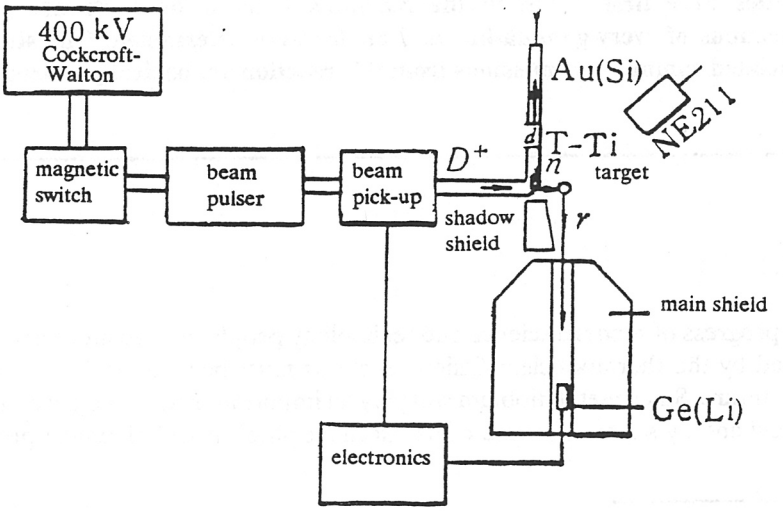

FIGURE 1. The sketch of the experimental set-up.

efficiency of the full energy peak of the Ge(Li) detector for gamma-ray with energy E_γ, N the number of atoms per unit area of the sample at the neutron incident direction, and f the correction factor for neutron flux and gamma-ray yields.

The experiments were carried out at a pulsed 400 kV Cockcroft-Walton accelerator at the Institute of Low Energy Nuclear Physics, Beijing Normal University. The experimental arrangement is shown in Fig.1, and the block diagram of electronics used in the measurements can be seen in Fig.2. The accelerator produces a 300 keV deuteron beam. When the beam passes through the pulsed system, a pulsed beam with a repetition frequency of 3.16 MHz and FWHM of pulse of 1 ns or so can be obtained. When the pulsed deuteron beam bombards the T(Ti) target, the pulsed neutron beams with an average energy of 14.9 MeV and an energy spread of 0.5 MeV are produced at 0° direction with respect to the deuteron beam. The average neutron intensity is about 5×10^8 neutrons/sec. The pulse signals are given by a capacitive beam current pick-up mounted on the

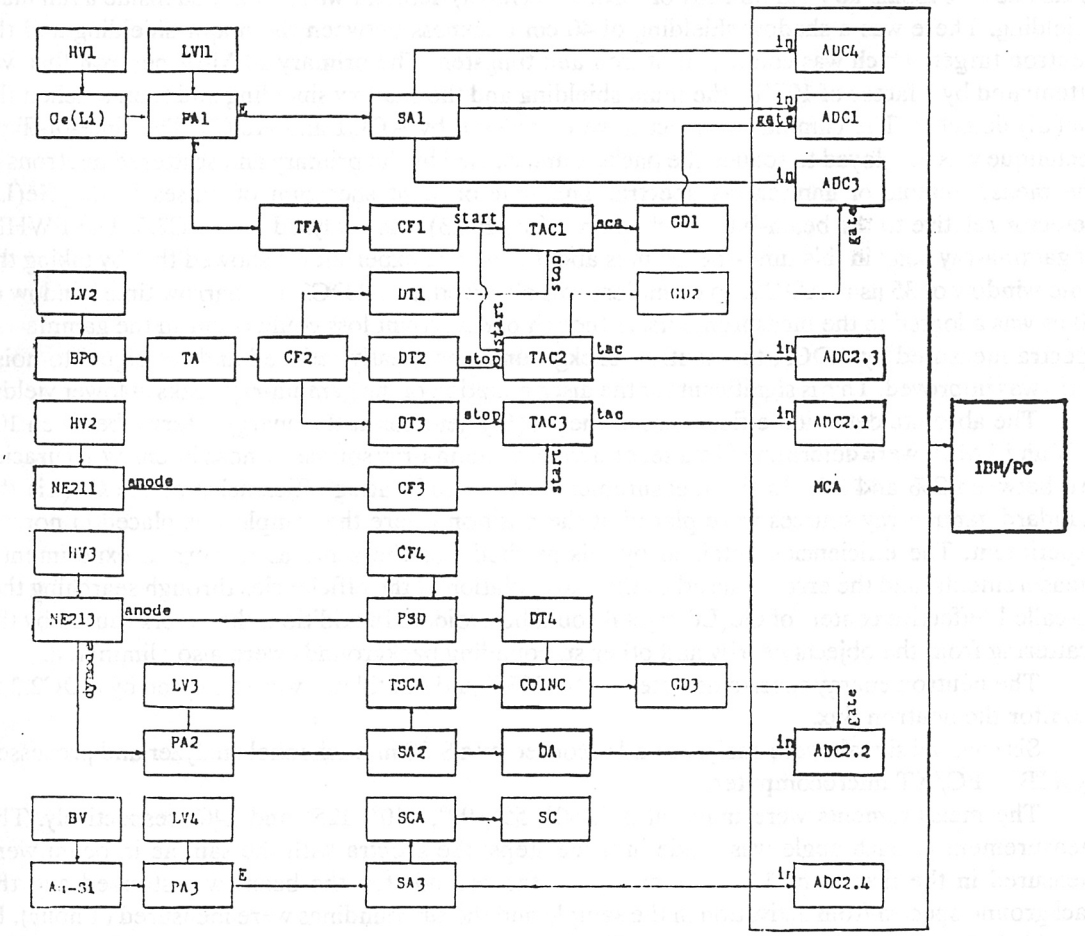

FIGURE 2 Electronic block diagram of data acquisition.

ADC—analog-digital converter, BV—bias voltage power supply, CF—constant fraction timing, DT—ns delay, FA—fast amplifier, GD—gate and delay generator, HV—high voltage power supply, LV—low voltage power supply, MCA—multichannel analyzer, PA—preamplifier, PSD—pulse shape discriminator, SA—spectroscopy amplifier, SC—scaler, SCA—single channel analyzer, TAC—time-amplitude converter, TFA—timing filtering amplifier, BPO—beam pickup, TSCA—timing single channel analyzer.

accelerator beam-line at a distance of 40 cm away from the neutron target. In addition, the time-of-flight spectrum of pulses in the plastic scintillator NE211 relative to the beam-burst pickup time, which was analysed by ADC2.3, was used to regulate and monitor the stability during the operation of the pulsed system.

The sample is a solid cylindrical metal niobium with a size of ϕ 3.02 × 3.044 cm and weight of 188 g. Its purity is more than 99.9%. The sample was placed at 13.4 cm ahead of the neutron target.

The neutron flux incident upon the sample was determined by the counts of the associated particle ^{4}He from $T(d, n)^4$He reactions. ^{4}He particles were measured by Au-Si detector at 90° angle to the deuteron beam axis and at 100 cm away from the neutron target. The associated particle energy-spectrum was analysed by ADC2.4.

The absolute gamma-ray yields were measured by a coaxial Ge(Li) detector placed at 139.4 cm away from the center of the sample. Its sensitive volume is 110.7 cm^3. Its energy resolution (FWHM) is 1.85 keV at 1332.5 keV gamma-ray of ^{60}Co. The Ge(Li) detector was positioned inside a full main shielding. There was a shadow shielding of 40 cm thickness between the major shielding and the neutron target, which was composed of iron and tungsten. The primary 14 MeV neutron flux was attenuated by a factor of 10^{-5} by the main shielding and the shadow shielding and then reached the Ge(Li) detector. The gamma-ray spectra were analysed by ADC1 and ADC3. The time-of-flight technique was employed to reduce the background caused by the primary and scattered neutrons in the measurements of gamma-ray spectra. The time-of-flight spectrum of pulses in the Ge(Li) detector relative to the beam-burst pickup time (see Fig.3) was analysed by ADC2.3. The FWHM of gamma-ray peak in this time-spectrum is about 7 ns. The experiments showed that by taking the time window of 35 ns in ADC1, no count loss was observed. For ADC3, the narrow time window of 20 ns was adopted in the measurements. Although partial count loss could occur in the gamma-ray spectra measured by ADC3, the neutron background was greatly reduced and the signal to noise ratio was improved. This is significant for the discrimination of the gamma-ray peaks at lower yields.

The absolute detection efficiencies of the Ge(Li) detector at the energy interval between 100 keV and 3 MeV were determined by a set of standard gamma-ray sources, whose intensity accuracies are between 2% and 3%. In the measurements of the calibrating efficiencies of the Ge(Li) the standard gamma-ray sources were placed at the position where the sample was placed in normal experiment. The efficiencies obtained by this method was the same as in normal experimental measurements, and the errors caused by the extrapolation of the efficiencies through searching the so-called "effective center" of Ge(Li) crystal could be avoided. In addition, the errors caused by the scattering from the objects nearby and other surrounding backgrounds were also eliminated.

The neutron energy spectra detected by NE213 liquid scintillator were analysed by ADC2.2 to monitor the neutron flux.

Six channel signals were analysed and recorded by a S-80 multichannel analyzer and processed by a IBM-PC/XT microcomputer.

The measurements were made at 30°, 40°, 55°, 90°, 110°, 125° and 140° respectively. The measurement at each angle was made in three steps: the spectra with the sample in beam were measured in the first step (12 hours or so). In the second step the beam was stopped and the background spectra from activation in the sample and the surroundings were measured (1 hour). In the third step the background spectra without sample in beam were measured (2 hours). The experiments proved that the detection efficiencies of the Ge(Li) detector were basically constant during the measurements at 7 different angles.

3. DATA HANDLING AND ANALYSIS

After net count N_α was obtained by the associated particle energy-spectrum analyzed by

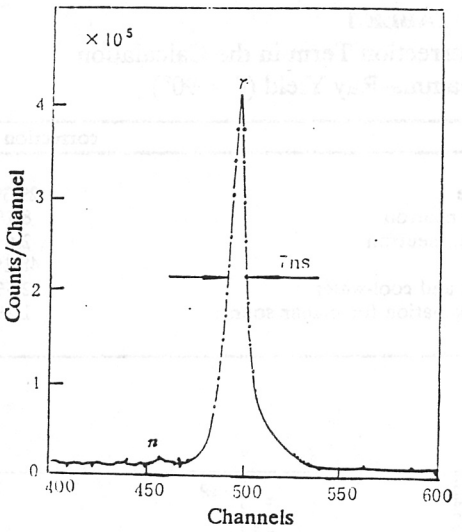

FIGURE 3 The time spectrum of pulses in the Ge(Li) detector relative to the beam-burst pickup time.

ADC2.4, the neutron numbers incident upon the sample could be obtained from the following formula:

$$\phi_n = \frac{\Omega_s N_\alpha}{\Omega_\alpha} A_\alpha \tag{2}$$

where Ω_α, Ω_s are the solid angles subtended by the associated particle detector and the sample with respect to the neutron target respectively, A_α is the anisotropic factor of neutron emission at 0° direction determined by the associated particle counts at 90° for $T(d, n)^4$He neutron source.

The area of the full energy peak of a gamma-ray was determined from the gamma-ray spectrum with the sample in beam subtracting the background spectrum without sample in beam (normalized by the associated particle counts) by means of a high resolution gamma-ray spectrum analysis program. After subtracting the activation background contribution of the corresponding gamma-ray peak from this area the net count N_γ was obtained. The quantitative calculations of the differential cross sections depended on the gamma-ray spectrum analysed by ADC1. The spectrum obtained by ADC3 was only used for reference in determining the peak positions of some weaker gamma-rays. The gamma-ray spectrum after subtracting the background spectrum without sample at 90° is shown in Fig. 4.

The neutron flux attenuation and the multiple scattering in the sample, the gamma-ray self-absorption in the sample, the neutron attenuation in the backing and cooling water of the neutron target, the solid angle correction caused by point approximation of the neutron source size etc. were considered in the calculations of the correction factor f. The calculation method of every correction can be found in Ref.[8]. The related neutron and gamma-ray data used in the calculations were taken from ENDF-BIV and Ref.[9]. As an example, every correction value to 934.4 keV gamma-ray is listed in Table 1.

TABLE 1
The Values of Each Correction Term in the Calculation of 934.40 keV Gamma-Ray Yield (θ = 90°)

correction factor	correction quantity
intensity attenuation of neutron in sample	29.3%
multiple scattering of elastically scattered neutron	8.1%
multiple scattering of inelastically scattered neutron	2.6%
absorption of γ-ray in sample	48.1%
attenuation of neutron in target substrate and cool-water	2.5%
solid angle correction due to point approximation for planar source	1.2%

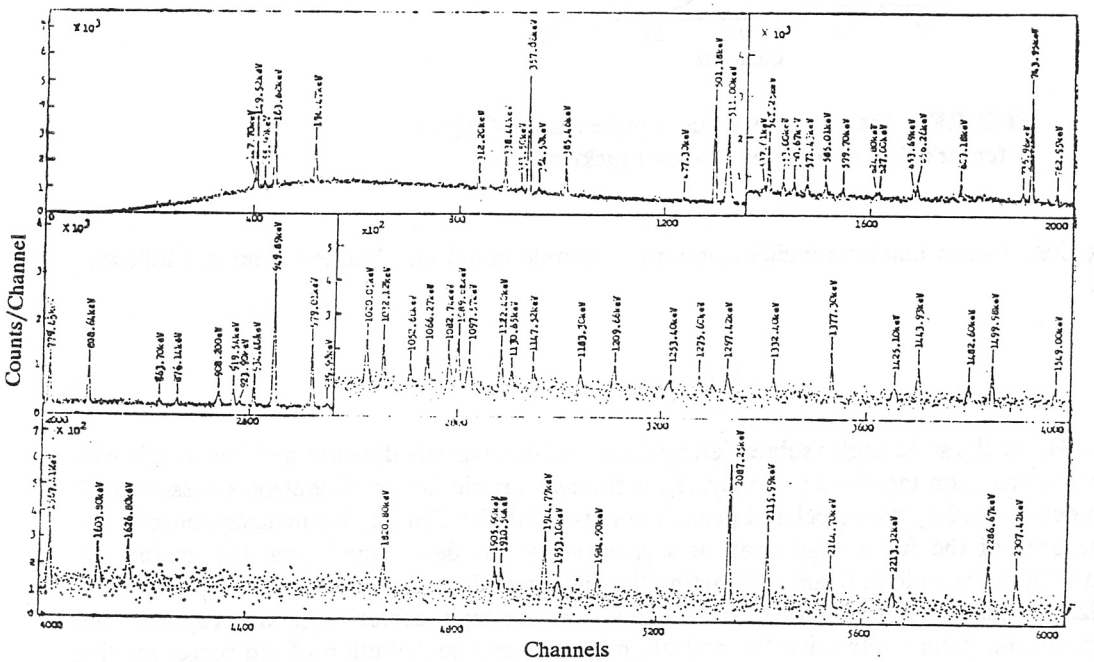

FIGURE 4 The gamma-ray spectrum in the reaction of 14.9 MeV neutrons with niobium sample (θ = 90°).

The errors of each factor in formula (1) were estimated as the following: The uncertainty of the neutron flux incident upon the sample ϕ_n was not more than 4%. The uncertainties of the absolute efficiencies of the Ge(Li) detector in the energy range from 100 keV to 2.6 MeV were between 1.5% and 2.5%. The uncertainties of the counts of the full energy peaks were determined by the statistical errors of each peak counts, there were larger differences for different gamma-ray peaks, in general, the uncertainties varied from 1% to 100%. The uncertainties of the correction factor f, which were introduced by the approximations of the correction calculation methods and the uncertainties of the neutron and gamma-ray cross section data used in the calculations, were between 1% and 3%.

The calculations of every correction and differential cross section were completed by GAM.FOR program.

TABLE 2

The Differential Cross Sections of the Gamma-Rays in the Reactions of 14.9 MeV Neutrons with Niobium

E_γ (keV)	reaction channel	transitions (keV)	differential cross sections (mb/sr)						
			30°	40°	55°	90°	110°	125°	140°
147.70	$(n,2n)$	2235.00—2086.67	3.22±0.55	2.97±0.48	3.37±0.54	3.10±0.47	3.17±0.63	3.15±0.47	3.07±0.41
149.52	$(n,2n)$	285.0—135.1	16.75±1.68	16.75±1.46	16.20±1.46	16.11±1.36	16.50±1.37	16.41±1.21	14.41±1.10
155.90	$(n,2n)$	1480.0—1324.0	0.832±0.250	0.864±0.260	0.690±0.210	0.693±0.180	0.890±0.220	0.789±0.200	0.744±0.190
163.68	$(n,2n)$	389.1—225.0	14.50±1.16	12.91±1.03	13.82±1.10	13.28±0.87	13.06±0.91	13.46±0.94	12.92±0.90
194.47	$(n,2n)$	479.6—285.0	7.57±0.68	7.78±0.62	7.50±0.67	7.30±0.47	7.67±0.54	7.00±0.56	6.44±0.45
318.20	(n,n')	1297.42—979.01							
		2003.38—1686.07	1.44±0.17	1.39±0.15	1.36±0.15	1.49±0.15	1.32±0.18	1.39±0.14	1.28±0.18
	$(n,2n)$	1642.0—1324.0							
338.44	(n,n')	1082.74—743.95	3.03±0.39	3.20±0.32	2.76±0.25	3.24±0.29	2.87±0.20	2.93±0.26	2.42±0.29
		2003.38—1665.76							
351.50	(n,n')	1686.07—1334.80	0.394±0.100	0.382±0.100	0.556+0.111	0.602±0.124	0.473±0.104	0.682±0.136	0.590±0.148
357.06	$(n,2n)$	357.06—0.0	19.85±1.40	19.02±1.33	19.53+1.36	19.16±0.96	17.86±1.07	18.09±1.08	18.36±1.06
364.50	(n,n')	1679.56—1315.08	0.654±0.196	0.648±0.194	0.531±0.159	0.511±0.128	0.414±0.104	0.470±0.117	0.453±0.113
385.46	(n,n')	1334.80—949.89	5.22±0.31	4.97±0.30	5.27±0.36	5.20±0.31	4.73±0.38	4.78±0.29	4.94±0.25
477.30	(n,n')	1968.25—1491.15	0.955±0.191	0.914±0.183	0.910±0.182	0.866±0.173	0.810±0.162	0.909±0.181	0.972±0.194
501.18	$(n,2n)$	501.18—0.0	18.31±1.10	18.78±1.13	20.13±1.21	19.54±1.24	18.92±1.04	18.69±1.03	18.34±1.03
537.61	(n,n')	2203.20—1665.76	0.511±0.153	0.416±0.125	0.401±0.120	0.405±0.121	0.369±0.111	0.467±0.140	0.371±0.111
541.25	(n,n')	1491.15—949.89	4.14±0.25	4.21±0.25	4.19±0.25	3.91±0.24	3.92±0.24	3.92±0.24	3.95±0.22
553.00	(n,n')	1297.42—743.95							
		1947.80—1394.61	1.19±0.18	1.30±0.20	1.16±0.12	1.23±0.17	1.15±0.15	0.990±0.120	0.990±0.150
	$(n,2n)$	1642.00—1089.00							

560.67	(n,n')	1369.41—808.64	1.47±0.18	1.60±0.19	1.81±0.18	1.25±0.17	1.29±0.13	1.56±0.12	1.44±0.14
571.43	(n,n')	1315.08—743.95	1.77±0.27	1.81±0.22	1.95±0.21	1.36±0.15	1.60±0.19	1.29±0.13	1.37±0.17
585.01	(n,n')	1394.61—810.05	1.10±0.17	1.16±0.17	1.27±0.19	1.23±0.18	0.951±0.143	0.899±0.135	1.08±0.16
599.70	(n,n')	2203.20—1603.80	0.695±0.201	1.14±0.22	1.36±0.41	0.773±0.155	1.12±0.22	1.21±0.36	0.916±0.275
		1682.82—1082.68							
624.80	(n,n')	1603.80—979.01	0.546±0.164	0.457±0.137	0.379±0.114	0.566±0.170	0.340±0.102	0.527±0.158	0.521±0.156
		2019.01—1394.61							
627.00	(n,n')	2118.59—1491.15	0.614±0.154	0.575±0.143	0.607±0.152	0.783±0.196	0.424±0.106	0.670±0.168	0.614±0.154
653.69	(n,n')	1603.80—949.89	1.07±0.13	1.31±0.16	1.11±0.13	1.13±0.14	0.936±0.112	1.06±0.13	0.888±0.106
656.26	(n,n')	686.44—30.40	1.75±0.18	1.87±0.19	1.97±0.18	1.51±0.16	1.90±0.17	1.75±0.18	1.65±0.17
689.18	(n,n')	2171.98—1483.37	2.05±0.23	1.86±0.15	2.18±0.20	1.86±0.19	2.08±0.17	1.97±0.18	1.95±0.20
736.96	(n,n')	1686.07—949.89	0.608±0.152	0.500±0.125	0.550±0.138	0.651±0.136	0.547±0.138	0.686±0.137	0.517±0.129
743.95	(n,n')	743.95—0.0	12.40±0.74	12.35±0.74	12.81±0.77	13.00±0.78	11.55±0.69	11.66±0.70	11.53±0.64
762.95	(n,2n)	2998.0—2235.0	0.920±0.110	1.12±0.13	1.04±0.12	1.11±0.13	1.14±0.13	0.930±0.112	0.917±0.110
		1738.0—975.0							
779.63	(n,n')	1728.59—949.89	5.00±0.35	5.31±0.37	5.00±0.35	5.01±0.35	4.48±0.31	4.70±0.33	4.24±0.41
		810.05—30.40							
808.64	(n,n')	808.64—0.0	4.68±0.35	4.43±0.33	4.67±0.35	4.96±0.35	4.35±0.33	4.42±0.30	4.67±0.29
863.70	(n,2n)	1089.0—225.3	0.631±0.158	0.629±0.189	0.632±0.190	0.871±0.174	0.636±0.159	0.606±0.152	0.600±0.180
876.14	(n,n')	2367.31—1491.15	0.916±0.147	0.932±0.158	1.27±0.19	1.00±0.16	0.889±0.135	0.877±0.263	0.803±0.201
908.20	(n,2n)	1410.2—501.18	2.70±0.24	2.62±0.21	2.65±0.21	2.72±0.27	2.59±0.20	2.84±0.23	2.50±0.28
919.54	(n,n')	949.89—30.40	2.98±0.22	3.04±0.24	2.83±0.21	2.86±0.22	3.06±0.23	2.75±0.19	2.89±0.23
		1728.59—808.64							
923.90			0.578±0.347	1.07±0.21	0.865±0.173	0.882±0.200	1.01±0.20	0.815±0.163	0.814±0.163

E_γ (keV)	reaction channel	transitions (keV)	differential cross sections (mb/sr)						
			30°	40°	55°	90°	110°	125°	140°
934.40	$(n,2n)$	1414.0—479.6	3.03±0.24	2.86±0.23	3.25±0.23	2.89±0.22	3.02±0.24	3.21±0.26	3.32±0.27
949.89	(n,n')	949.89—0.0	20.36±1.22	20.50±1.23	20.93±1.26	19.22±1.11	18.61±1.09	18.60±1.12	18.83±1.06
		2203.20—1253.40							
979.01	(n,n')	979.01—0.0	9.01±0.54	9.20±0.55	9.56±0.57	9.43±0.56	9.31±0.56	9.18±0.55	8.98±0.60
989.90	(n,n')	1968.25—979.01	0.421±0.105	0.556±0.139	0.505±0.126	0.496±0.124	0.420±0.105	0.510±0.128	0.570±0.143
1020.05	(n,n')	1968.25—949.89	2.03±0.20	2.41±0.24	2.09±0.15	2.20±0.21	2.20±0.20	2.44±0.17	2.02±0.22
1032.12	(n,n')	2367.31—1334.80	1.76±0.18	1.75±0.18	1.32±0.13	1.69±0.17	1.44±0.14	1.59±0.16	1.52±0.15
		2329.90—1297.32							
1052.66	(n,n')	1082.74—30.40	0.885±0.133	1.04±0.16	0.942±0.141	0.995±0.149	0.882±0.149	0.922±0.138	0.821±0.123
1066.27			1.87±0.19	2.02±0.16	2.04±0.20	2.00±0.18	1.84±0.17	1.72±0.19	2.02±0.18
1082.74	(n,n')	1082.74—0.0	1.61±0.16	1.71±0.17	1.43±0.10	1.69±0.10	1.69±0.17	1.48±0.11	1.64±0.18
1089.62	(n,n')	2171.98—1082.74	2.13±0.21	2.40±0.24	2.45±0.20	2.39±0.21	2.14±0.21	2.40±0.17	2.16±0.22
1097.57			1.56±0.16	1.71±0.17	1.61±0.11	1.66±0.15	1.48±0.15	1.53±0.15	1.48±0.15
1122.40			1.76±0.19	2.02±0.20	2.10±0.17	2.00±0.16	1.86±0.19	2.02±0.18	2.00±0.18
1130.65	$(n,2n)$	1632.00—501.18	1.12±0.28	1.08±0.27	1.13±0.28	1.02±0.25	0.872±0.218	1.14±0.28	1.05±0.26
1147.52	(n,n')	2482.89—1334.80	1.23±0.22	1.19±0.18	0.973±0.117	0.872±0.131	1.13±0.17	0.874±0.131	1.11±0.17
1183.30	(n,n')	2133.20—949.89	0.642±0.130	0.839±0.126	0.852±0.128	0.859±0.112	0.694±0.104	0.918±0.119	0.840±0.160
1209.66	(n,n')	2019.01—808.64	1.18±0.18	1.19±0.18	1.31±0.20	1.16±0.20	1.02±0.15	1.24±0.19	1.06±0.16
1253.40	(n,n')	1253.40—0.0	0.926±0.185	1.10±0.22	0.871±0.139	0.800±0.160	0.804±0.168	0.865±0.138	0.964±0.241
1275.60	$(n,2n)$	1411.0—135.1	—	0.630±0.189	0.582±0.175	0.514±0.154	0.470±0.141	0.637±0.191	0.618±0.215
1297.42	(n,n')	1297.42—0.0	0.995±0.150	0.993±0.150	1.13±0.17	1.08±0.16	0.933±0.140	1.05±0.16	1.09±0.21
1332.40	(n,n')	2019.01—686.44	1.00±0.20	0.966±0.193	0.987±0.148	1.07±0.13	1.00±0.20	1.02±0.15	0.967±0.193

1377.30			2.63±0.24	2.41±0.20	2.48±0.20	2.35±0.19	2.45±0.22	2.75±0.25	2.48±0.24
1425.10			0.548±0.110	0.650±0.130	0.528±0.106	0.588±0.110	0.532±0.110	0.536±0.107	0.551±0.110
1443.93	$(n,2n)$	1945.0—501.18	1.62±0.15	1.76±0.18	1.70±0.15	1.74±0.13	1.58±0.14	1.76±0.16	1.49±0.22
1482.60	(n,n')	1482.60—0.0	0.877±0.210	0.967±0.222	1.07±0.18	0.921±0.138	0.766±0.191	0.918±0.156	0.897±0.179
1499.98	(n,n')	1499.98 —0.0	1.93±0.19	1.96±0.20	2.14±0.15	1.91±0.15	1.78±0.18	2.09±0.16	2.00±0.20
1549.00			0.634±0.159	0.741±0.185	0.982±0.246	0.871±0.235	0.626±0.125	0.676±0.203	0.545±0.164
1567.41	(n,n')	1567.41—0.0	1.91±0.25	1.93±0.25	1.74±0.23	1.89±0.20	1.65±0.17	2.10±0.25	1.98±0.21
1603.80	(n,n')	1603.80—0.0	0.355±0.178	0.322±0.161	0.556±0.278	0.366±0.186	0.229±0.115	0.465±0.233	0.316±0.108
1626.80			0.896±0.179	0.811±0.195	0.698±0.175	0.780±0.230	0.738±0.185	0.784±0.188	0.915±0.229
1820.80			0.713±0.178	0.809±0.162	0.809±0.162	0.838±0.210	0.659±0.132	0.852±0.174	0.770±0.193
1905.90			0.671±0.134	0.764±0.153	1.00±0.20	1.17±0.23	1.01±0.20	0.908±0.182	0.740±0.148
1910.50	(n,n')	1910.50—0.0	0.493±0.148	0.619±0.186	0.712±0.142	0.963±0.193	0.600±0.120	0.726±0.145	0.558±0.120
1944.79	$(n,2n)$	1944.79—0.0	1.59±0.24	1.65±0.21	1.95±0.20	1.71±0.19	1.52±0.15	1.85±0.19	1.72±0.34
1953.10			0.535±0.161	0.622±0.187	0.811±0.162	0.503±0.146	0.494±0.148	0.503±0.151	0.675±0.203
1984.90			0.427±0.128	0.551±0.165	0.478±0.143	0.522±0.157	0.567±0.170	0.470±0.141	0.450±0.135
2087.25	$(n,2n)$	2087.25—0.0	6.48±0.42	6.82±0.44	7.21±0.48	7.00±0.45	6.95±0.40	7.13±0.46	6.55±0.43
2115.99			2.57±0.26	2.56±0.31	2.39±0.24	2.69±0.30	2.64±0.26	2.78±0.28	2.46±0.25
2164.70	(n,n')	2164.70—0.0	1.26±0.26	1.29±0.26	1.64±0.16	1.32±0.16	1.44±0.20	1.51±0.15	1.33±0.27
2213.32			1.06±0.27	1.10±0.28	1.34±0.40	0.920±0.276	1.07±0.27	1.11±0.33	0.855±0.210
2286.67	$(n,2n)$	2286.67 —0.0	2.94±0.24	3.12±0.25	2.83±0.20	2.59±0.29	2.65±0.21	3.00±0.24	2.95±0.31
2307.42			1.13±0.22	1.43±0.28	1.20±0.24	1.48±0.22	1.12±0.22	1.45±0.22	1.02±0.21
2407.35			0.757±0.227	0.787±0.236	0.814±0.244	0.852±0.256	0.825±0.248	0.472±0.236	0.824±0.412
2432.28			0.662±0.199	0.609±0.183	0.839±0.252	0.757±0.227	0.700±0.210	0.879±0.264	0.730±0.219
2507.50			0.669±0.167	0.683±0.171	0.770±0.193	0.814±0.163	0.635±0.159	0.959±0.240	0.724±0.217

4. RESULTS AND DISCUSSIONS

The differential gamma-ray production cross sections at the 7 angles for the reactions of 14.9 MeV neutrons with niobium are listed in Table 2. In comparison with the results measured at 90° in Ref.[8], the energy resolution of the spectrometer has been improved. In the present measurement, because the energy width per channel analysed by the multichannel analyzer is changed from 0.8 keV to 0.4 keV, the 149.52 keV gamma-line is split into two lines of 147.70 keV and 149.52 keV respectively. In addition, through comparisons among the gamma-ray spectra measured at 7 angles, 1286.63 keV, 1967.36 keV and 2128.52 keV given in the past measurement at 90° are deleted, and the 155.90 KeV and 599.70 keV gamma-lines are newly discerned. Therefore there are still 79 gamma-lines. In these spectrum lines about 40 lines are first observed in the reactions induced by neutrons.

The possible reaction types and transitions of 62 gamma-lines are also given in Table 2 according to the known level scheme [3,10]. Of course, these are only the preliminary results. It must depend on more experiments such as the measurements of excitation curves, gamma-gamma coincidences and so on to determine the position of every spectrum line in the level scheme of the corresponding nuclide correctly.

The angular distributions of the differential production cross sections of 12 gamma-lines with

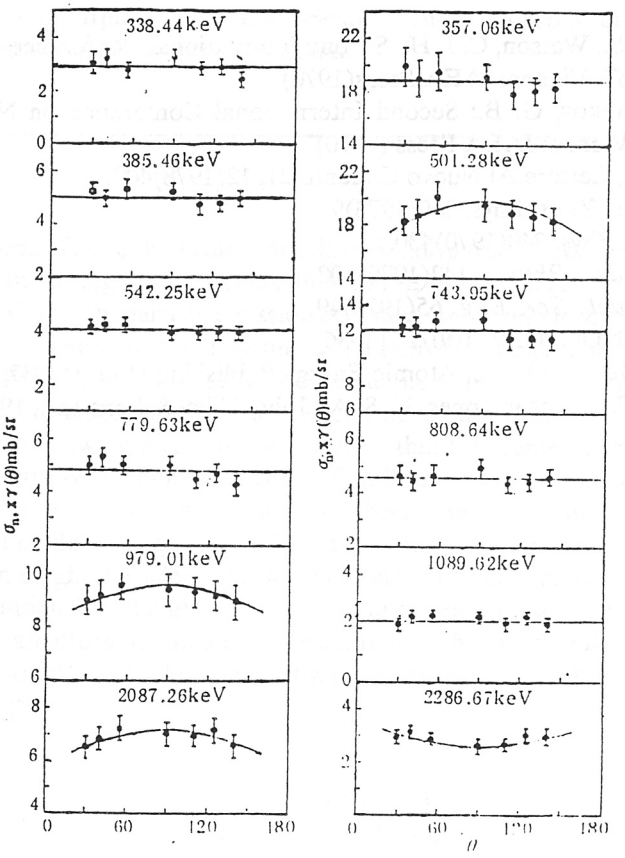

FIGURE 5. The angular distributions of differential cross sections of some gamma-lines in the reactions of 14.9 MeV neutrons with niobium sample.

TABLE 3
The Coefficients of Legendre Polynomial to Fit the Angular Distributions of Differential Cross Sections for Some Gamma-Lines

E_γ (keV)	B_0(mb/sr)	B_2(mb/sr)
501.18	18.91±0.42	1.78±0.80
979.01	9.23±0.21	0.69±0.39
2087.25	6.88±0.17	0.66±0.32
2287.67	2.85±0.09	0.48±0.18

higher yields are shown in Fig.5, in which 8 lines are basically isotropic, and for the other 4 ones the cross sections show some regular but smaller variations with angles. Legendre polynomial is used for fitting these distributions. The fitting coefficients are listed in Table 3.

REFERENCES

[1] Crocker, V. S., Blow, S., Watson, C. J. H.: Second International Conference on Nuclear Data for Reactors, Vol. 1, 67, Vienna: IAEA Press(1970).
[2] Chernilin, Yu. F., Yankov, G. B.: Second International Conference on Nuclear Data for Reactors, Vol. 1, 49, Vienna: IAEA Press (1970).
[3] U. Abbondanno et al., Lettere Al Nuovo Cimento 21, 12(1978)409.
[4] I. J. van Heerden et al., Zeits. Phys. 260(1973)9.
[5] H. Gobel et al., Zeits. Phys. 240(1970)430.
[6] V. C. Rogers et al., *Nucl. Phys.* A142(1970)100.
[7] D. W. Drake et al., *Nucl. Sci. Eng.* 65(1978)49.
[8] Zhou Hongyu et al., INDC (CPR) 010/L, (1986).
[9] Liu Yingzang et al., Decay Scheme, Atomic Energy Publishing House, 1982, p.477.
[10] D. M. Lederer et al., Table of Isotopes, U. S. A., John Wiley & Sons Inc., 1978, p.379.